Judd M. Cahoon,[1] Ruju R. Rai,[1] Lara S. Carroll,[1] Hironori Uehara,[1] Xiaohui Zhang,[1] Christina L. O'Neil,[2] Reinhold J. Medina,[2] Subtrata K. Das,[1] Santosh K. Muddana,[1] Paul R. Olson,[1] Spencer Nielson,[1] Kortnie Walker,[1] Maggie M. Flood,[1] Wyatt B. Messenger,[1] Bonnie J. Archer,[1] Peter Barabas,[1] David Krizaj,[1] Christopher C. Gibson,[3] Dean Y. Li,[4] Gou Y. Koh,[5] Guangping Gao,[6] Alan W. Stitt,[2] and Balamurali K. Ambati[1]

Intravitreal AAV2.COMP-Ang1 Prevents Neurovascular Degeneration in a Murine Model of Diabetic Retinopathy

Diabetes 2015;64:4247–4259 | DOI: 10.2337/db14-1030

Diabetic retinopathy (DR) is the leading cause of blindness in the working-age population in the U.S. The vision-threatening processes of neuroglial and vascular dysfunction in DR occur in concert, driven by hyperglycemia and propelled by a pathway of inflammation, ischemia, vasodegeneration, and breakdown of the blood retinal barrier. Currently, no therapies exist for normalizing the vasculature in DR. Here, we show that a single intravitreal dose of adeno-associated virus serotype 2 encoding a more stable, soluble, and potent form of angiopoietin 1 (AAV2.COMP-Ang1) can ameliorate the structural and functional hallmarks of DR in Ins2Akita mice, with sustained effects observed through six months. In early DR, AAV2.COMP-Ang1 restored leukocyte-endothelial interaction, retinal oxygenation, vascular density, vascular marker expression, vessel permeability, retinal thickness, inner retinal cellularity, and retinal neurophysiological response to levels comparable with nondiabetic controls. In late DR, AAV2.COMP-Ang1 enhanced the therapeutic benefit of intravitreally delivered endothelial colony-forming cells by promoting their integration into the vasculature and thereby stemming further visual decline. AAV2.COMP-Ang1 single-dose gene therapy can prevent neurovascular pathology, support vascular regeneration, and stabilize vision in DR.

Diabetes affects 25.8 million people in the U.S., and its prevalence is expected to triple in the next 20 years (1). Diabetic retinopathy (DR) is the leading cause of blindness in the working-age population (2). The leading cause of vision loss in DR is diabetic macular edema (DME), a condition in which fluid accumulates underneath the central macula due to a breakdown of the blood retinal barrier (BRB).

Current treatments for DME include laser photocoagulation, intravitreal agents that block vascular endothelial growth factor (VEGF), and/or intravitreal corticosteroids. Such treatments address the downstream consequences but not the vascular endothelial cell loss and ischemia underlying DME (3). Moreover, these therapies improve vision in only a minority of patients (4). Merely 23–33% of patients treated with ranibizumab (5) and 34% of patients treated with aflibercept (6) achieve significant visual gains. Because it creates small burns that can interfere with peripheral vision and overall visual performance, traditional treatment with laser photocoagulation is primarily used to retard rather than reverse retinal nonperfusion (7). Intravitreal steroids have served as an alternative for patients who have contraindications or are resistant to anti-VEGF agents but are inferior to VEGF

[1]Department of Ophthalmology and Visual Sciences, John A. Moran Eye Center, University of Utah, Salt Lake City, UT
[2]Centre for Vision and Vascular Science, Queen's University Belfast, Belfast, Ireland
[3]Department of Biomedical Engineering, University of Utah, Salt Lake City, UT
[4]Program in Molecular Medicine, Department of Medicine, University of Utah, Salt Lake City, UT
[5]Korean Advanced Institute for Science and Technology, Daejeon, South Korea
[6]Department of Molecular Genetics and Microbiology, University of Massachusetts, Worcester, MA

Corresponding author: Balamurali K. Ambati, bala.ambati@utah.edu.

Received 3 July 2014 and accepted 23 August 2015.

This article contains Supplementary Data online at http://diabetes.diabetesjournals.org/lookup/suppl/doi:10.2337/db14-1030/-/DC1.

R.R.R. and H.U. are co–second authors.

inhibitors in recovering visual acuity and are associated with side effects like cataract and intraocular hypertension (8). Given the suboptimal outcomes, we developed a different approach to DME focusing on the reversal of retinal vascular damage and restoration of normal perfusion.

The underlying pathogenesis of DR is largely due to hyperglycemia (9). Hyperglycemia triggers an inflammatory response leading to leukocyte adhesion, microvascular occlusion, and consequent hypoxia (10,11). Further, hyperglycemia instigates pericyte loss, compromising endothelial stability and BRB integrity. Eventual capillary degeneration leads to retinal nonperfusion, exacerbating retinal hypoxia (12). Consequent pathological VEGF-induced angiogenesis is uncoordinated and results in immature, leaky vessels with inadequate perfusion, creating a vicious cycle of hypoxia-driven VEGF secretion and DME (13). Retinal ganglion cell (RGC) loss, neuronal dysfunction, and changes in vision are also seen in patients with DR, concurrently with vascular pathology (14). Hence, as a therapeutic goal, vascular stabilization could promote normal perfusion of metabolically demanding retinal neurons and thereby avert the sight-threatening sequelae of ischemia and hyperpermeability.

One therapeutic target is angiopoietin 1 (Ang1), a vascular growth factor that has an abnormally low concentration in the vitreous of patients with DR (15). Ang1, via binding to the Tie2 endothelial receptor, fosters vessel quiescence and maturation and suppresses vascular leakage by preventing VEGF-induced degradation of vascular endothelial (VE)-cadherin, a transmembrane protein in the adherens junction between endothelial cells that promotes vascular integrity and decreases vascular permeability (16,17). Ang1 also promotes the survival of damaged vascular endothelial cells through the phosphatidylinositol 3-kinase/Akt cascade (18). Thus, restoration of Ang1 signaling could serve as a possible solution for preventing endothelial loss, retinal ischemia, and abnormal VEGF expression in DR (19).

Pharmaceutical development of Ang1 as a viable therapy has been hindered by its insolubility and aggregation. Ten years ago, a novel, stable, soluble and more potent version of Ang1, cartilage oligomeric matrix protein Ang1 (COMP-Ang1), was bioengineered to overcome the limitations of native Ang1 (20). Although the benefits of COMP-Ang1 have been demonstrated for vasculopathic disorders in animal models of the cardiac (21), nervous (22), and renal (23) systems, this study is the first to test its effectiveness for the prevention and treatment of DR.

We hypothesized that, if introduced early in diabetes, constitutive expression of COMP-Ang1 via adeno-associated virus serotype 2–mediated gene therapy (AAV2.COMP-Ang1), either as a monotherapy or in combination with human-derived endothelial colony-forming cells (ECFCs), could protect retinal neurovascular structure and function in a type 1 diabetic Ins2Akita mouse model of DR. We found that COMP-Ang1 prevents the endothelial loss, capillary dropout, BRB instability, leukocyte dysfunction, neuroretinal attenuation, and visual decline associated with DR. In addition, COMP-Ang1 enhances the therapeutic efficacy of ECFCs in mitigating DR through vascular and visual rehabilitation.

RESEARCH DESIGN AND METHODS

Mice

This research protocol was approved by the Institutional Animal Care and Use Committee of the University of Utah and conforms to the standards in the Associaton for Research in Vision and Ophthalmology Statement for the Use of Animals in Ophthalmic and Vision Research. The diabetic C57BL/6-Ins2^{Akita}/J (Ins2Akita) mouse and its background wild-type (WT) strain, C57BL6/J, were used (24). Mice heterozygous for the *Ins2* mutation experience progressive retinal abnormalities 12 weeks after the onset of hyperglycemia, including apoptosis (i.e., endothelial and RGC loss) and functional deficits (increased vascular permeability and decreased neuronal function) (25).

Mice were randomly assigned to one of three experimental groups: AAV2.COMP-Ang1, AAV2.AcGFP (*Aequorea coerulescens* green fluorescent protein), or PBS. At 2 months of age (Supplementary Fig. 3), each mouse was anesthetized by injection of 1.25% tribromoethanol (Sigma-Aldrich, St. Louis, MO) at a dose of 0.025 mL/g body wt i.p. Each mouse was treated with either 2 μL AAV2 solution (2.0×10^9 particles) or PBS injected into the vitreous cavity of both eyes with a 33-gauge microsyringe (Hamilton Company, Reno, NV). An additional cohort of mice was treated as described above at 6 months of age. Two weeks later, this cohort received a second intravitreal injection with 1 μL of 1×10^5 ECFCs (Supplementary Fig. 3).

Virus Vector Construction

The plasmids pAAV.COMP-Ang1 and pAAV.AcGFP were created by incorporating the COMP-Ang1 cDNA from the pCMV-dhfr2-COMP-Ang1 (donated generously by the Koh Laboratory, KAIST, Daejeon) into pAAV-MCS (Agilent Technologies, Santa Clara, CA), while pAAV.AcGFP was created by the same technique with AcGFP cDNA from the pIRES2-AcGFP1 plasmid (Clontech Laboratories, Mountain View, CA) (Supplementary Fig. 3).

For in vivo assays requiring imaging with the Spectralis HRA+OCT (Heidelberg Engineering, Heidelberg, Germany), mice were anesthetized by an inhalation of 3% isoflurane/O_2 mixture in a closed canister at a flow rate of 1.0 Lpm. Pupils were dilated with a 1% tropicamide.

Retinas were harvested and processed for in situ hybridization (ISH) according to standard protocols using procedures to avoid RNAse contamination.

RT-PCR for COMP-Ang1 mRNA Expression

Primer sequences for COMP-Ang1 (University of Utah Gene Core, Salt Lake City, UT) were as follows: COMP-Ang1 F 5′-GCTCTGTTTTCCTGCTGTCC-3′ and COMP-Ang1 R 5′-GTG ATGGAATGTGACGCTTG-3′. Primer sequences for the internal control, GAPDH, were as follows: GAPDH F 5′-AACTTTGGG ATTGTGGAAGGG-3 and GAPDH R 5′-ACCAGTGGATGCAGG GATGAT-3′G.

Immunoprecipitation and Western Blot

Retinas were harvested and protein lysate samples were immunoprecipitated with anti-FLAG M2 affinity gel (Sigma-Aldrich). Eluted proteins samples were run on 12% SDS-PAGE. Overall protein levels were compared with anti-GAPDH (1:3,000; Abcam, Cambridge, MA) and anti–β-actin (1:3,000; Abcam). Samples were tested for anti–VEGF-A (1:200; Santa Cruz Biotechnology, Santa Cruz, CA), anti–VE-cadherin (1:1,000, Abcam), and anti–phospho-Src (PY419, 1 μg/mL; R&D Systems, Minneapolis, MN).

Immunofluorescence of Retinal Flat Mounts for Vascular Markers

Enucleated globes were fixed in 4% paraformaldehyde followed by retinal dissection. Specimens were stained with 1:200 α-smooth muscle actin antibody or neuron-glial antigen 2 antibody conjugated with cyanine dye (Cy3) (Sigma-Aldrich) and 5 μg/mL Alexa Fluor 647–conjugated isolectin GS-IB4 (Invitrogen) in blocking buffer overnight at 4°C. After washing, the retina was flat mounted on a glass slide. Full retinal field immunofluorescence (IF) images were captured at low magnification, followed by increasing magnification of each quadrant with scanning laser confocal microscopy (Olympus America).

Trypsin Digest for Retinal Vascular Architecture

Enucleated globes were fixed in 2% formalin. The retina was detached around the subretinal space. The optic nerve was cut under the disc. The specimen was digested at 37°C in 2.5% trypsin/0.2 mol/L TRIS at pH 8.0 for 30–60 min. Specimens were transferred to distilled water and to 0.5% triton X-100 surfactant/distilled water and left at room temperature for another hour. Lastly, the specimen was moved to 0.1% triton X-100/distilled water for mounting and dried in a 37°C incubator. Samples were stained with periodic acid Schiff staining and imaged with light microscopy (Olympus, Center Valley, PA). Acellular capillaries and pericytes were counted in each of a total of five high-powered fields per retinal quadrant.

Transendothelial Electrical Resistance for BRB Integrity

In vitro measurements of transendothelial electrical resistance (TER) were performed with an electrical cell substrate impedance sensing (ECIS) system (Applied Biophysics, Troy, NY). Human retinal microvascular endothelial cells (HrMVECs) (Cell Systems, Kirkland, WA) were seeded (50,000 cells/well) onto fibronectin-coated gold microelectrodes in ECIS culture wells (8W10E+; Applied Biophysics) and incubated overnight at 37°C in complete medium (EBM-2 plus EGM2-MV supplements, Lonza Group, Basel, Switzerland) until cell resistance reached a plateau. Cells were serum starved for 1 h until resistance was stabilized (1,200 Ω). Each well received one of three experimental treatments: COMP-Ang1 protein (Enzo Life Sciences, Farmingdale, NY), VEGF protein (R&D, Minneapolis, MN), or PBS. Monitoring was continued for 21 h. The data from triplicate wells were averaged and presented as normalized resistance versus time.

Miles Assay for Retinal Vasopermeability

Mice were administered Evans blue (EB) (Sigma-Aldrich) at a dosage of 20 mg/kg through tail vein injection. After 4 h, the vasculature was perfused with PBS. The retinas were next harvested and placed in formamide at 70°C for 18 h. Samples were centrifuged for 2 h at 40,000*g* in a 0.2-μm filter. EB concentration was detected spectrophotometrically by subtracting absorbance at 620 nm from 740 nm.

Acridine Orange Fluorography for Leukocyte Transendothelial Migration

Acridine orange (Acros Organics, Geel, Belgium) (0.10%/PBS) was filtered with a 0.22-μm filter. The solution (0.05 mL/min for a total of 1 min) was injected into the tail vein. Imaging used Spectralis HRA+OCT (Heidelberg Engineering) with a 488-nm argon blue laser with a standard 500-nm long-pass filter. Images were acquired from both eyes with a 55-degree lens using the movie mode on the Spectralis HRA+OCT.

Flow Assay for Leukocyte-Endothelial Interaction

HrMVECs were cultured in parallel-plate fibronectin-coated flow chambers (μ-Slide VI 0.4, ibidi USA, Madison, WI) until 80% confluent and exposed to tumor necrosis factor-α (TNF-α) (10 ng/mL) (R&D Systems) or vehicle control for 3 h. Human leukocytes were isolated as previously described in accordance with Institutional Review Board guidelines (26) and diluted in warmed ultrasaline (Lonza Group) to 1×10^6 cells/mL. Leukocytes were pumped through the parallel plate flow chambers using a syringe pump (Harvard Apparatus, Holliston, MA) at 1 dynes/cm^2 (typical venous shear stress). Differential interference contrast images were acquired at a rate of 1/s for 1 min, and the number of leukocytes adhered to or rolling on the monolayer was quantified as leukocytes/frames/second. Three independent flow wells were averaged to attain the reported values.

Immunoperoxidase Staining for Retinal Hypoxia

Mice received an intraperitoneal injection of the bioreductive hypoxia marker pimonidazole (Hypoxyprobe, Burlington, MA) at 60 mg/kg (3). Three hours later, retinas were harvested and stained with a hypoxyprobe-1 monoclonal antibody conjugated to fluorescein isothiocyanate to detect reduced pimonidazole adducts (Hypoxyprobe) forming in $pO_2 < 10$ mmHg.

Optical Coherence Tomography for Retinal Thickness

Mice were imaged bilaterally with optical coherence tomography (OCT) (Spectralis HRA+OCT, Heidelberg Engineering). Retinal cross-sectional thickness was measured 250 μm relative to the optic nerve head, using the en face image as a guide. Measurements were recorded for each retinal quadrant and averaged to attain the reported values.

Microsphere Fluorescence for Retinal Vasopermeability

Each mouse received a dosage of 100 μL/20 g tail vein injections with 100 nm microspheres (Magsphere, Pasadena, CA) conjugated to either the near-infrared fluorophore ZW800 (Flare Foundation, Boston, MA) (4) or GFP (Magsphere). Bilateral imaging by Spectralis HRA+OCT (Heidelberg Engineering) was performed with fluorescein angiography (FA) and indocyanine green modalities.

Immunofluorescence for Retinal Thickness and VE-Cadherin

Enucleated globes were fixed in 4% paraformaldehyde. The globes were cut in 10-μm sections and stained with anti–VE-cadherin antibody (1:200, Abcam) and DAPI (Sigma-Aldrich). Sections were captured with scanning laser confocal microscopy (Olympus America).

Immunofluorescence of Retinal Flat Mounts for RGC Density

Four-month-old mice received intravitreal injections of either AAV2.COMP-Ang1 or PBS as described above. Six months later, retinas were fixed and dissected as described above for flat mounts. Specimens were labeled with 1:200 pan-Brn3 antibody (Santa Cruz Biotechnology), followed by Alexa Fluor 546–conjugated secondary antibody (Invitrogen), and counterstained with DAPI (Sigma-Aldrich). Eight fields were imaged for each retina using the confocal ×40 oil objective; these comprised four evenly spaced fields (one per quadrant) adjacent to the optic nerve and four fields (similarly spaced) near the flat mount periphery. Images were counted blind by two separate investigators. Counts were averaged for each retina and compared across control and experimental groups.

Electroretinography for Retinal Function

Mice were dark adapted, anesthetized with ketamine/xylazine (90 mg/10 mg/kg body wt), and placed on a controlled warming plate (TC-1000; CWE Instruments, Ardmore, PA) (5). Electroretinograms (ERGs) were taken between a gold corneal electrode and a stainless steel scalp electrode with a 0.3- to 500-Hz band-pass filter (UTAS E-3000; LKC Technologies, Gaithersburg, MD). The photoflash unit was calibrated to deliver 2.5 cd s/m^2 at 0 dB flash intensity, and scotopic measurements were recorded with flash intensities increasing from 0.0025 to 250 cd s/m^2. The b-wave amplitudes were determined in scotopic conditions, and the mean values at each stimulus intensity were compared with an unpaired two-tailed *t* test.

Optokinetic Tracking for Visual Acuity

Optomotor reflex-based spatial frequency threshold tests were conducted in a visuomotor behavior measuring system (OptoMotry, CerebralMechanics, Lethbridge, AB, Canada). Tracking was defined as a reproducible smooth pursuit with a velocity and direction concordant with the stimulus. Trials of each direction and spatial frequency were repeated until the presence or absence of the tracking response could be established unequivocally. Rotation speed (12°/s) and contrast (100%) were kept constant.

ECFCs

Fresh human cord blood, donated under full ethical approval by healthy volunteers at the Northern Ireland Blood Transfusion Service (Belfast, U.K.), underwent density gradient fractionation for the isolation of mononuclear cells and was selected for ECFCs via resuspension in complete medium (EBM-2 plus EGM-2 MV supplements, Lonza Group) supplemented with 10% FBS and seeding onto 24-well culture plates precoated with rat tail collagen type 1 (BD Biosciences, Bedford, U.K.) at a density of 1×10^7 cells/mL. Cells were labeled (Qtracker 655, Invitrogen, Life Technologies, Carlsbad, CA) per the manufacturer's instructions.

Immunofluorescence of Retinal Flat Mounts for ECFC Engraftment

From the mice that had received intravitreal ECFCs, harvested retinas were fixed and dissected as described above for flat mounts (Supplementary Fig. 3*B*). Specimens were stained with 5 μg/mL Alexa Fluor 647–conjugated isolectin GS-IB4 (Invitrogen) and mounted on a glass slide as described above. ECFC integration was counted in four high-powered fields in each retinal quadrant.

Scratch Assay for ECFC Migration

ECFCs were plated on rat-tail collagen-coated sixwell plates prelabeled with traced lines (27). When cells were 90% confluent, a uniform straight scratch was made in the monolayer using a 200-μL pipette tip. After injury, cells were washed, medium was changed, and reference photographs were taken within each region marked by the lines using a phase contrast microscope (Eclipse E400, Nikon, Tokyo, Japan). Wells were incubated with the experimental treatment (doses of COMP-Ang1 protein from 0–1,000 ng/mL), and images were captured at hourly intervals. Endothelial cell migration was quantified by calculating the proportion of denuded area.

Matrigel Assay for ECFC Tubulogenesis

ECFCs were labeled with a fluorescent dye (PKH Cell Linker kit for General Cell Membrane Labeling, Sigma-Aldrich) as previously described (28). Next, they were suspended in growth factor reduced basement membrane matrix (Matrigel, Becton Dickinson Biosciences, Franklin Lakes, NJ), and 50-μL aliquots were spotted onto a 24-well plate. Spots were covered with DMEM containing 5% porcine serum and treated with either control or increasing doses of COMP-Ang1. After 24 h, wells were assessed for the presence of tubules. Images were acquired by using a laser confocal microscope (Nikon).

Statistical Analysis

All numerical data were analyzed in Excel (Microsoft, Redmond, WA) and presented as the mean ± SD. Student two-tailed *t* test, with α level 0.05, was used to compare differences between two samples. ANOVA test, with

$P < 0.05$, followed by Tukey post hoc analysis, was used to compare differences between four groups.

RESULTS

Intravitreal AAV2 Gene Therapy Is Safe for the Mouse Retina

The long-term safety of intraocular AAV-mediated gene therapy has been validated by numerous animal and human studies in which vector inoculation was well tolerated and unaccompanied by any structural or functional defects (29). We recently reported that the intraocular injection of exogenous AAV2 constructs did not impact retinal thickness, influence ERG responses, or increase the risk of retinochoroidal apoptosis (30). Concordant with prior results, the current study found no significant differences ($P = 0.3$ at -30 dB, 0.6 at 0 dB, and 0.6 at 20 dB) in scotopic and photopic b-wave amplitudes on ERG between WT mice treated with intravitreal AAV2.COMP-Ang1, AAV2.AcGFP, or PBS (Supplementary Fig. 1*A*). Furthermore, optokinetic tracking (OKT) response of no-injection WT control mice did not change appreciably compared with PBS-treated mice ($P = 0.5$) over the course of 5 weeks (Supplementary Fig. 1*B*).

Intravitreal AAV2.COMP-Ang1 Expresses COMP-Ang1 in the Mouse Retina

AAV2 localization and transfection in the retina were confirmed by in vivo and ex vivo detection of the fluorescent gene product of the sham viral control by confocal microscopy; further, COMP-Ang1 mRNA and protein expression was verified by ex vivo immunoassay.

AcGFP fluorescence was initially observed at 1 week postinjection and persisted through to the 4 months postinjection end point (Supplementary Fig. 2*A*). As anticipated based on previous experience with intravitreal AAV2 (31), AcGFP signal was visualized in all retinal quadrants at the level of the ganglion cell–inner plexiform layer (GC-IPL) (Supplementary Fig. 2*B* and *C*).

COMP-Ang1 production in the mouse retina was demonstrated via semiquantitative RT-PCR (Supplementary Fig. 2*D*), ISH (Supplementary Fig. 2*F–H*), and immunoblotting (Supplementary Fig. 2*E*) at the 4 months postinjection end point. In parallel with AcGFP fluorescence, ISH revealed increased amounts of COMP-Ang1 mRNA in the inner retina, predominantly in the GC-IPL (Supplementary Fig. 2*F–H*).

COMP-Ang1 Prevents Breakdown of Vascular Structure

The principal morphologic features of DR are pericyte, endothelial cell, and capillary dropout (32). Concordantly, retinal vessel density was discernably reduced in IF and trypsin digest images of Ins2Akita control (PBS and AAV2.AcGFP) versus WT retinas (Fig. 1*A–C*). Endothelial cell ($P < 0.01$) (Fig. 1*D*) and pericyte ($P < 0.01$) (Fig. 1*E*) coverage was significantly decreased in the diabetic controls compared with WT, while capillary acellularity was increased ($P < 0.01$) (Fig. 1*F*).

IF and trypsin digest images of AAV2.COMP-Ang1 exhibit an improvement in vessel density compared with diabetic controls (Fig. 1*A–C*), accompanied by a significant drop in acellular capillary density ($P < 0.01$ vs. AAV2.AcGFP, $P < 0.01$ vs. PBS, and $P < 0.01$ vs. WT) (Fig. 1*F*). AAV2.COMP-Ang1 significantly rescued endothelial cell loss relative to controls (WT 23.2%, AAV2.COMP-Ang1 20.5%, PBS 15.5%, AAV2.AcGFP 15.3%, $P < 0.01$) (Fig. 1*D*) but not pericyte coverage (WT 6.5%, AAV2.COMP-Ang1 3.8%, PBS 4.3%, AAV2.AcGFP 3.9%, $P = 0.9$) (Fig. 1*E*).

Previous reports have demonstrated that the rescue of pericytes, the major source of endogenous Ang1 in the capillary unit (33), is not necessary for Ang1 rescue of function as long as Ang1 is available in adequate quantities (34). Our data suggest that in lieu of pericytes, AAV2.COMP-Ang1 can provide sufficient Ang1 endothelial trophic signaling to prevent capillary dropout (Fig. 1*F*).

COMP-Ang1 Promotes BRB Integrity

Ischemia from capillary dropout in DR stimulates VEGF production and consequent vascular hyperpermeability (3). Accordingly, the TER of HrMVECs decreased after treatment with VEGF compared with PBS in vitro ($P < 0.01$) (Fig. 2*A*), while EB extravasation was elevated in PBS- and AAV2.AcGFP-treated diabetic controls (3.8- and 3.1-fold, respectively) (Fig. 3*A*) compared with WT mice ($P < 0.01$). Microsphere leakage was similarly elevated in diabetic controls (Fig. 3*B*).

COMP-Ang1 significantly increased the TER ($P < 0.01$) (Fig. 2*A*) of HrMVECs and decreased EB extravasation ($P < 0.01$) (Fig. 3*A*) and microsphere (Fig. 3*B*) leakage in diabetic mice.

These results indicate that COMP-Ang1 restores the barrier function of the retinal vasculature in DR. To explore the molecular underpinnings of this finding, we investigated the influence of COMP-Ang1 on VEGF-A, the proto-oncogene nonreceptor tyrosine kinase Src, and the intercellular junction adhesion molecule VE-cadherin. VEGF-A is known to induce vessel leakage in DR through Src-mediated downregulation of VE-cadherin, while Ang1 is known to upregulate VE-cadherin (16,35).

COMP-Ang1 decreased Src phosphorylation (Fig. 2*B*) and increased VE-cadherin expression in HrMVECs (Fig. 2*C*). Both Ins2Akita and WT retinas treated with AAV2.COMP-Ang1 had reduced levels of VEGF-A (Fig. 2*D* and Supplementary Fig. 4) and increased levels of VE-cadherin (Fig. 2*E* and Supplementary Fig. 4).

Ang1 acts on the phosphatidylinositol 3-kinase/Akt cascade to prevent the apoptosis of damaged vascular endothelial cells (18). Considering the reduction in capillary acellularity and endothelial cell loss with COMP-Ang1, we explored Akt phosphorylation as a possible mechanism for COMP-Ang1–mediated survival of endothelial cells.

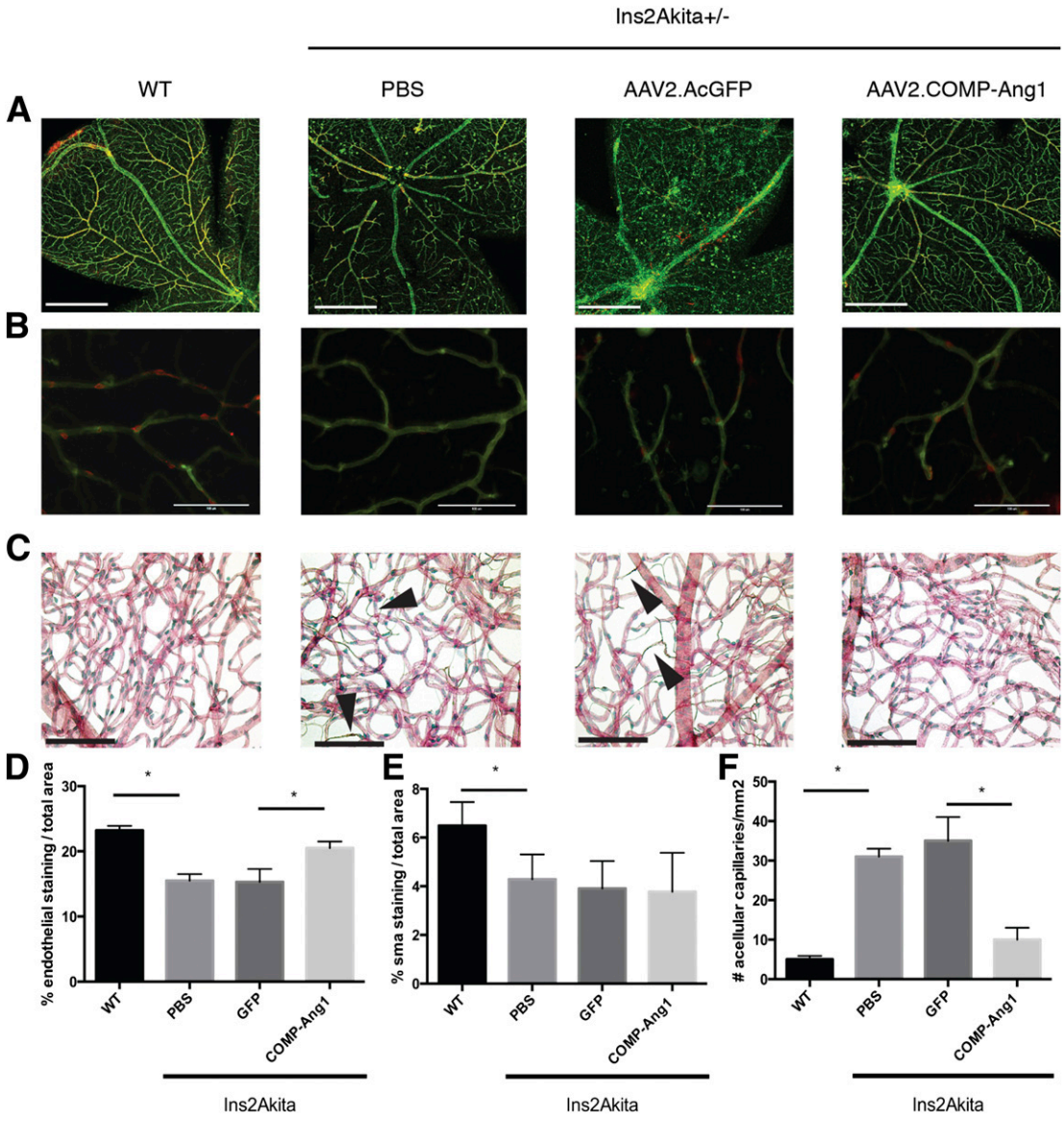

Figure 1—AAV2.COMP-Ang1 mitigates diabetic retinal capillary dropout. *A*: Representative retinal flat mounts prepared from 6-month-old mice and stained for isolectin (endothelial cell marker [green]) and α-smooth muscle actin (smooth muscle marker [red]). *B*: Magnified view of retina stained with isolectin and neuron-glial antigen 2 (pericyte marker). Ins2Akita mice experienced pericyte and endothelial dropout; the latter was prevented with a single intravitreal dose of AAV2.COMP-Ang1. *C*: Trypsin digest featuring retinas representative of each group. Black arrowheads denote acellular capillaries. Quantification using ImageJ of endothelial coverage (*D*) and pericyte coverage (*E*). *F*: Acellular capillaries were manually counted and averaged over an area 1 mm^2. Eight eyes were used in each analysis. Data are mean ± SD. *$P < 0.01$, ANOVA. Post hoc comparisons with a Tukey test to compare means of each group. Scale bars = 600 μm (*A*), 100 μm (*B*), and 200 μm (*C*).

COMP-Ang1 increased Akt phosphorylation at the serine 473 residue in both ECFCs and human umbilical vein endothelial cells (Fig. 2*F*).

COMP-Ang1 Reduces Leukocyte-Endothelial Adhesion and Leukostasis

DR is characterized by a chronic subclinical inflammatory response that is thought to play a critical role in its pathogenesis (36). The less deformable and more activated leukocytes in DR are conjectured to contribute to retinal nonperfusion and capillary dropout through increased attachment to endothelial cells and entrapment within the capillaries (37).

Leukocyte adhesion to the vascular wall is mediated, in part, by TNF-α (38). Correspondingly, the endothelial monolayer of HrMVECs exposed to TNF-α experienced an abnormally high rate of leukocyte adherence. Treatment with COMP-Ang1 protein decreased the number of adherent leukocytes per minute by 80% ($P < 0.01$) (Fig. 2*G*).

On Acridine orange leukocyte fluorography (39), leukocyte rolling was significantly elevated in Ins2Akita control (9.8 cells/min) versus WT retinas (3 cells/min, $P < 0.01$)

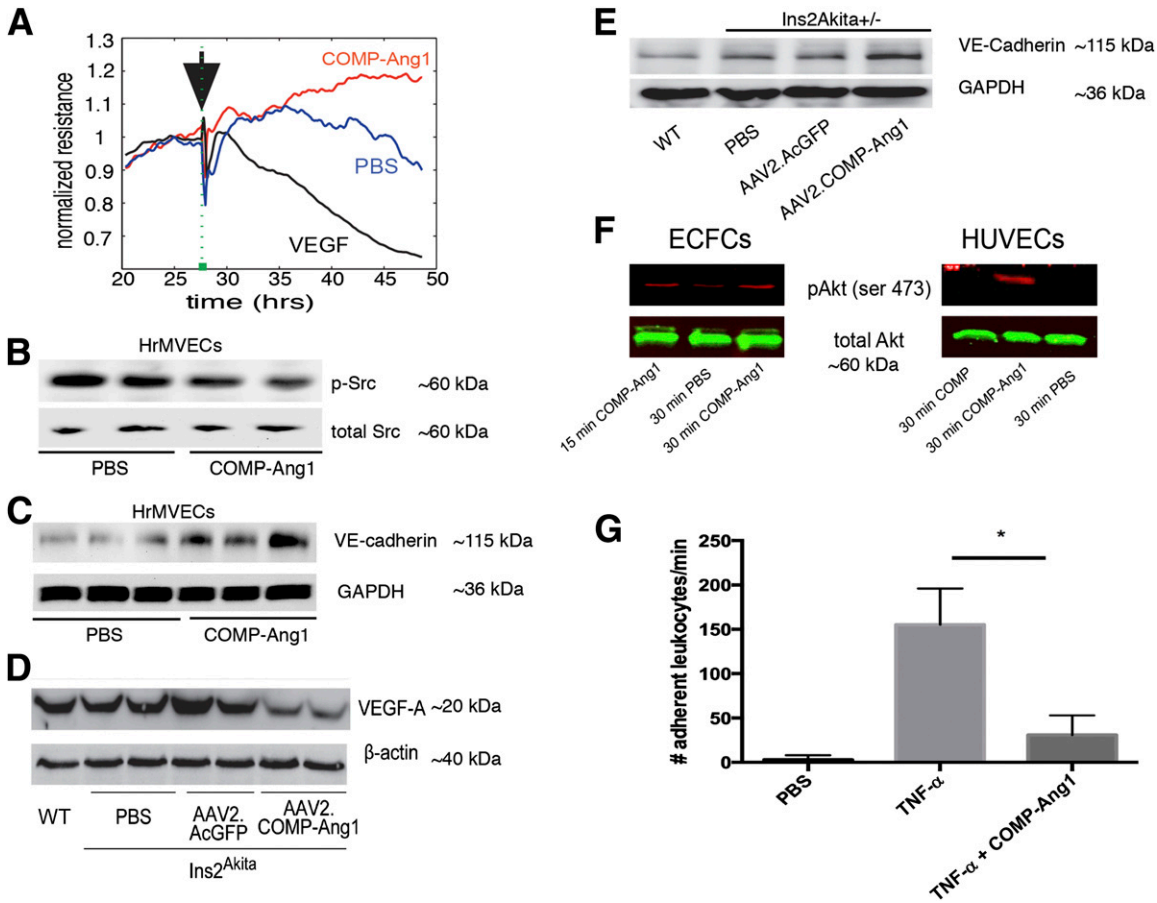

Figure 2—COMP-Ang1 increases endothelial integrity. *A*: Representative graph of ECIS of HrMVECs with COMP-Ang1 (100 ng/mL), VEGF (50 ng/mL), or control (PBS) added to the media. COMP-Ang1 increased resistance of HrMVECs (n = 3). Increases in endothelial resistance were correlated with deceased Src phosphorylation (*B*) and increased VE-cadherin (*C*) in HrMVECs as demonstrated by Western blot (n = 3). Western blot from Ins2Akita mouse retinas demonstrating decreased VEGF-A (*D*) and increased VE-cadherin (*E*) in mice treated with AAV2.COMP-Ang1. COMP-Ang1 increased Akt phosphorylation at the serine 473 residue in both ECFCs and human umbilical vein endothelial cells (HUVECs). *G*: COMP-Ang1 reduced TNF-α–induced leukocyte rolling in cultured HrMVECs (n = 6 per group). *P < 0.01, ANOVA. hrs, hours.

(quantitative image Fig. 3*C* and representative image Fig. 3*D* with white arrows pointing to leukocyte aggregations at the bifurcation). AAV2.COMP-Ang1 was able to reduce this rate to below the disease-free baseline (2.8 cells/min, $P < 0.01$) (Fig. 3*C* and Supplementary Videos 1–4).

These results indicate that the improvement in vascular parameters by COMP-Ang1 may have an anti-inflammatory component.

COMP-Ang1 Reduces Hypoxia

Leukostasis has been proposed as a mechanism of capillary nonperfusion and retinal hypoxia (40). Since hypoxia is a potent inducer of VEGF-A, we further assessed the relationship between COMP-Ang1 and hypoxia. Pimonidazole staining was increased in the diabetic control mice relative to WT mice, whereas it was reduced nearly to baseline levels in AAV2.COMP-Ang1 mice (Fig. 3*E*).

Collectively, our outcomes demonstrate a pathway for COMP-Ang1–mediated retinal vascular functional stabilization. The inhibition of leukocyte adhesion and stimulation of Akt phophorylation lead to the preservation of perfusion and normalization of tissue oxygenation, whereas the inhibition of VEGF-A and Src phosphorylation lead to the preservation of VE-cadherin and normalization of permeability.

COMP-Ang1 Prevents Retinal Neuronal Dysfunction

DR causes neural degeneration of the inner retina (14). Consistent with this, the retinas on OCT and IF images from Ins2Akita control mice (185 μm) were qualitatively and quantitatively thinner than in WT mice (210 μm, $P < 0.01$) (Fig. 4*A–D*). In parallel, GC-IPL cell density was also decreased in Ins2Akita control (68 nuclei/300 μm length) versus WT (45 nuclei/300 μm length) retinas ($P < 0.001$) (Fig. 4*B–D*), a 34% loss of cells.

AAV2.COMP-Ang1 preserved retinal thickness (WT 210 μm, AAV2.COMP-Ang1 205 μm, AAV2.AcGFP 181 μm, and PBS 185 μm; $P < 0.01$) (Fig. 4*A* and *D*) and prevented loss of cells in the GC-IPL (65 nuclei/300 μm length; $P = 0.03$) in Ins2Akita mice (Fig. 4*B–D*).

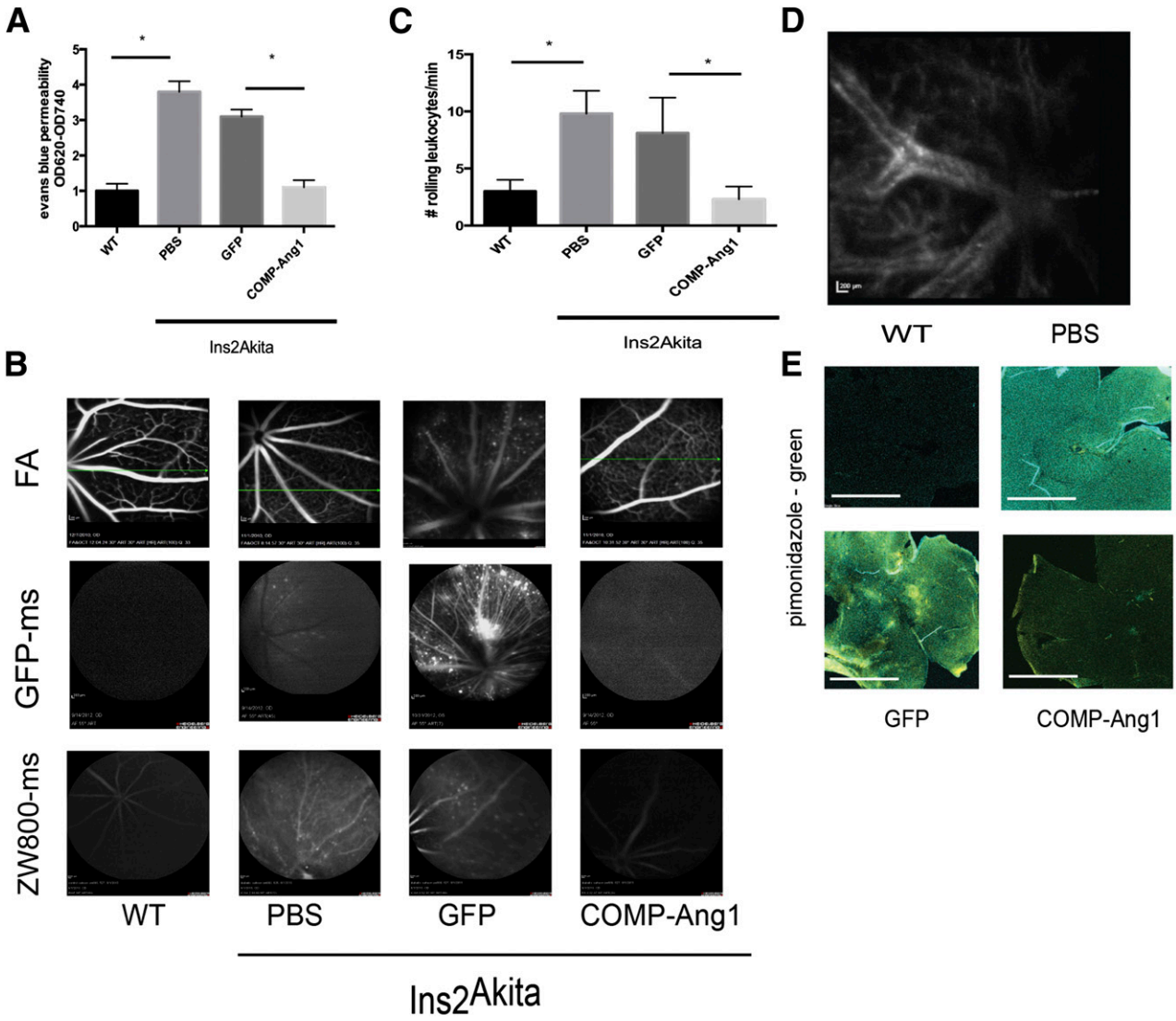

Figure 3—COMP-Ang1 enhances vascular barrier function and reduces retinal hypoxia in the diabetic retina. *A*: EB extravasation from the retina of Ins2Akita mouse was increased compared with control; treatment with AAV2.COMP-Ang1 returned vascular hyperpermeabilty to control levels. Eyes from eight mice were used in each analysis; data are mean ± SD. **P* < 0.01 compared with WT, **P* = 0.02 compared with AAV2.AcGFP. *B*: FA did not reveal any leakage in diabetic mice; however, with GFP or the near-infared fluorophore ZW800 conjugated to aminated latex microspheres (GFP-ms or ZW800–ms; 100 nm in diameter), in vivo leakage was captured using the FA or indocyanine green (ICG) imaging modality on Spectralis, respectively. Note that background GFP fluorescence of the AAV2.AcGFP-treated diabetic mice masked signal from the GFP microspheres. *C*: Diabetes induced leukocyte rolling in the retinal vasculature, as captured by acridine orange leukocyte fluorography. *D*: Representative image of acridine orange leukocyte fluorography with white arrowheads pointing to adherent and rolling leukocytes. COMP-Ang1 prevents leukostasis and inflammation in this model of diabetic retinopathy. (See also Supplementary Video 1.) *E*: Representative retinas (four mice per group) from mice treated with hypoxyprobe (pimonidazole). COMP-Ang1 reduced hypoxia in diabetic mouse retinas. Scale bars: 600 μm (*E*). **P* < 0.01, ANOVA. Post hoc comparisons with a Tukey test to compare means of each group.

Further characterization of GC-IPL cells with the RGC-specific marker Brn3 revealed no difference in RGC counts within the central retinas of PBS versus COMP-Ang1–treated Ins2Akita mice ($P = 0.7$) (Fig. 4*E*). However, peripheral retinas showed a 17% loss of ganglion cells (Fig. 4*F*). Although this difference was not statistically significant ($P = 0.07$), the trend shows an effect size similar to that reported for RGC loss in the peripheral retina of diabetic versus WT mice (41), suggesting that a larger sample size would provide sufficient power to confirm an effect.

In sum, these data suggest that AAV2.COMP-Ang1 is beneficial in preventing diabetes-induced GC-IPL atrophy and peripheral RGC cell loss but may also target or recruit non-RGC cell types within the inner retina for neuroprotection.

COMP-Ang1 Prevents Visual Dysfunction

Patients with DR manifest with visual deficits early in the disease, and animals exhibit changes in visual acuity and contrast sensitivity through impaired visual tracking behavior and delayed retinal electrical responses (42). In

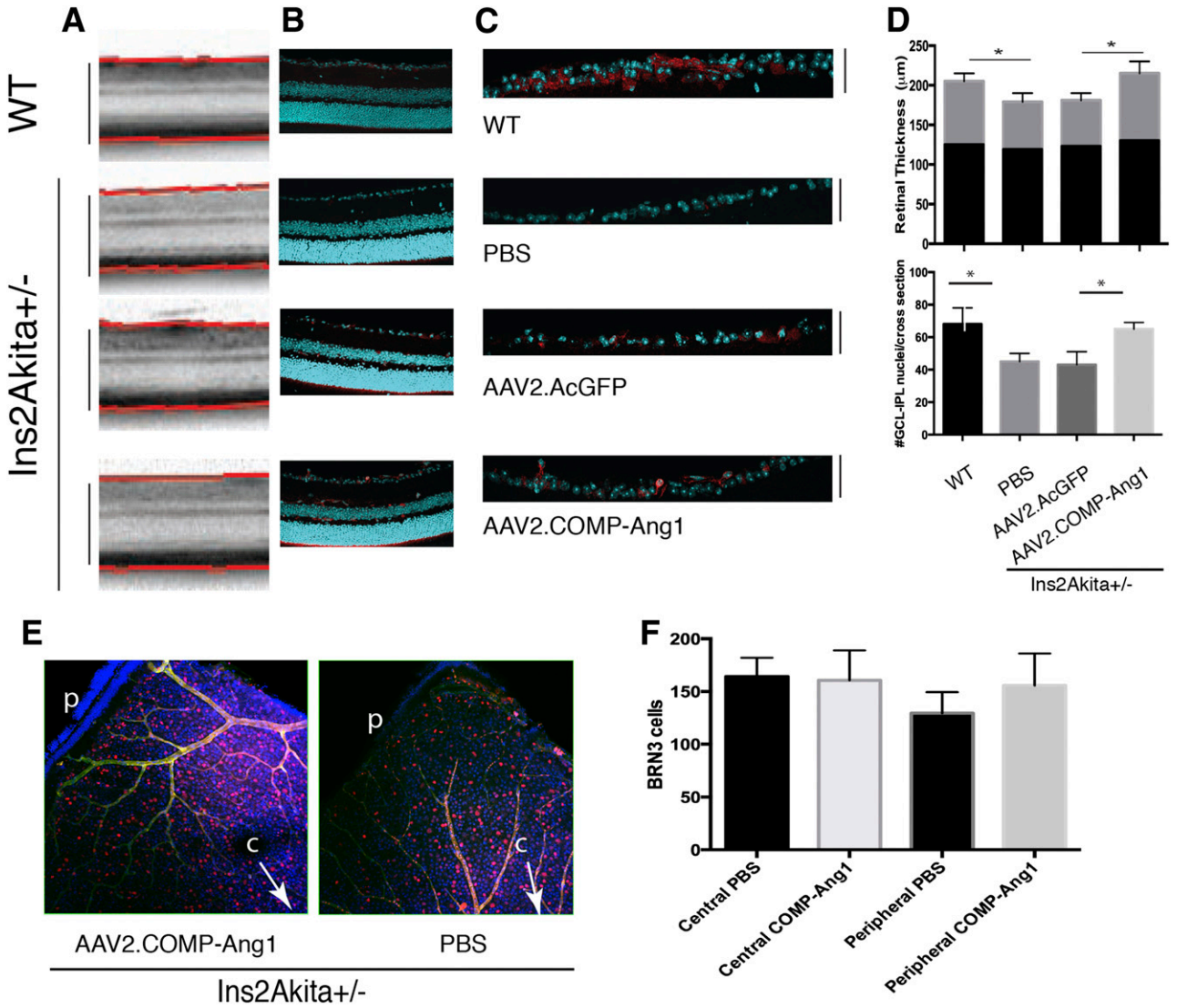

Figure 4—AAV2.COMP-Ang1 prevents diabetes-induced GC-IPL degeneration. *A*: Representative figures from OCT measuring retinal thickness. The red line, generated by OCT software, indicates the retinal surface and Bruch membrane. Scale bars = 200 μm. *B*: Cross-sections of 6-month-old retinas from WT or Ins2Akita mice treated with PBS, AAV2.AcGFP, or AAV2.COMP-Ang1 stained with DAPI. *C*: View of the GC-IPL from mice stained for VE-cadherin (red) or nuclei (DAPI, blue) demonstrating increased VE-cadherin and nuclear staining. Scale bars = 30 μm (right). *D*: Quantification of retinal thickness from OCT showing that AAV2.COMP-Ang1 prevented diabetes-induced retinal thinning as measured in vivo (*P < 0.01 vs. both WT and AAV2.AcGFP). AAV2.COMP-Ang1 prevented diabetes-induced inner retinal layer loss (*P = 0.03, ANOVA with post hoc Tukey test) as measured by nuclei counted in the GC-IPL in retinal cross-sections. *E*: Representative retinal flat mounts stained with BRN3 (red [a marker for retinal ganglion cells]), isolectin (green [marker for vessels]), and DAPI (blue). Qualitatively, fewer peripheral RGCs are observed in PBS-treated Akita retina. *F*: Ins2Akita mice showed no difference in central RGCs with either treatment, but there was a trend toward reduced peripheral RGCs in PBS-treated mice vs. COMP-Ang1–treated mice (17% fewer ganglion cells in PBS group [P = 0.07]). At least six eyes from each group were tested. Data are mean ± SD. *P < 0.01, ANOVA. Post hoc comparisons with a Tukey test to compare means of each group. c, central; p, peripheral.

line with this, ERG and OKT responses were within normal limits for WT mice but abnormally depressed in diabetic control mice (at −40 dB, WT 127 μvolts, PBS = 57 μvolts, and AAV2.AcGFP 73 μvolts, $P < 0.01$; at 4 months postinjection, WT = 0.388 cycles/degree, PBS = 0.184 cycles/degree, and AAV2.AcGFP = 0.174 cycles/degree, $P < 0.01$) (Fig. 5*A–C*).

AAV2.COMP-Ang1 treatment diminished the dampening in scotopic b-wave amplitudes (185 μvolts, $P < 0.01$) (Fig. 5*A* and *B*) caused by anomalous photoreceptor-bipolar communication in DR (43). Likewise, Ins2Akita mice treated with AAV2.COMP-Ang1 were able to avert the deterioration of OKT (0.312 cycles/degree; $P < 0.01$) (Fig. 5*C*).

Together, spatial resolution and ERG data show that AAV2.COMP-Ang1 can preserve retinal neurophysiological function.

COMP-Ang1 Enhances ECFC Treatment Effect

The recellularization and resultant refunctionalization of acellular capillaries could theoretically halt the nonperfusion at the root of DR pathophysiology, but in diabetes

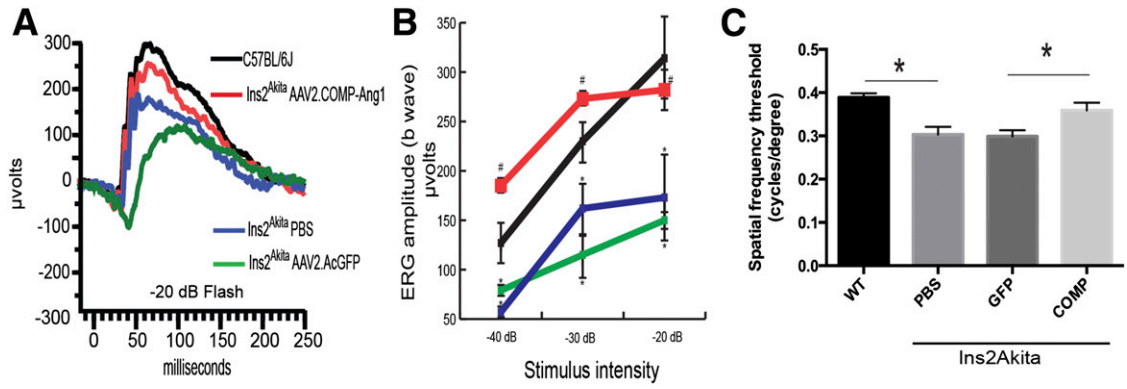

Figure 5—AAV2.COMP-Ang1 prevents diabetes-induced neural dysfunction. *A*: Representative example of ERG response from all groups of mice. Electrical retinal response was elicited, and the amplitude of b-wave during scotopic conditions at −3.62 log (Cd s/m^2) (−40 dB), −2.62 log (Cd s/m^2) (−30 dB), and −1.62 log (Cd s/m^2) (−20 dB) intensity was recorded. *B*: Decreased amplitudes were recorded in Ins2Akita mice treated with PBS or AAV2.AcGFP compared with WT mice, and AAV2.COMP-Ang1 prevented the decrease in amplitude. **P* < 0.01, ANOVA; #*P* < 0.01, compared with AAv2.AcGFP. Assessing visual acuity was accomplished by testing optomotor tracking response of Ins2Akita mice treated with AAV2.COMP-Ang1 or control compared with WT. *C*: Ins2Akita mice exhibited decreased optokinetic tracking response (measured as cycles/degree). AAV2.COMP-Ang1 (COMP) prevented the decrease in visual response; at least six mice from each group were tested. Data are mean ± SD. **P* < 0.01, ANOVA. Post hoc comparisons with a Tukey test to compare means of each group.

the endogenous reparative cells responsible for this task have a decreased ability to associate with existing vascular networks (44). The exogenous delivery of human-derived ECFCs, as evidenced by their utility in oxygen-induced retinopathy (45), may be able to compensate for this deficiency but have not yet been explored in the context of DR. We know that ECFCs express high levels of the Ang1 receptor, Tie2 (46), and that Ang1 promotes the differentiation of stem cells into vasculogenic cells for vessel engraftment and reformation. Therefore, we tested the regenerative potential of dual therapy with COMP-Ang1 and ECFCs.

COMP-Ang1 demonstrated a dose-dependent increase in 6-h migration (2.5-fold increase over control at 10 ng/mL, $P < 0.01$) (Fig. 6*A*) and 24-h tubulogenesis (4.3-fold over control, $P < 0.01$) (Fig. 6*B*) of ECFCs in vitro, as assessed by scratch migration assay and matrigel tube formation assay, respectively. In vivo, aged 26-week-old Ins2Akita mice treated with AAV2.COMP-Ang1 had increased 72-h ECFC vessel integration on confocal microscopy (Fig. 6*C* and Supplementary Videos 5 and 6) and 2-month visual response with OKT (AAV2.COMP-Ang1 = 0.307 cycles/degree, AAV2.AcGFP = 0.251 cycles/degree, and PBS = 0.263 cycles/degree; $P < 0.01$) (Fig. 6*D*).

Our results show that COMP-Ang1 boosts the capacity of ECFCs to rebuild vessels and counteract vision loss in DR.

DISCUSSION

This study established the salutary effects of COMP-Ang1 in ameliorating pivotal pathogenic events in the trajectory toward DME through neurovascular normalization. Structural and functional indices of neurovascular restoration to a state more consistent with a homeostatic disease-free phenotype by COMP-Ang1 included endothelial and capillary density; vessel permeability; VEGF-A, phospho-Src, VE-cadherin, and phospho-Akt levels; leukocyte-endothelial interaction and retinal hypoxia; neuroretinal thickness, GC-IPL cellularity, and peripheral RGC density; and most importantly, vision. Furthermore, COMP-Ang1 augmented the effectiveness of ECFCs in regenerating vessels and stabilizing vision in advanced DR. Based on these results, our working model for further study centers on the premise of COMP-Ang1 directly or indirectly suppressing inflammation and modulating the actions of VEGF, Src, VE-cadherin, and Akt at the molecular level, thereby influencing downstream processes of perfusion and BRB reinforcement vital for neurovascular stability.

Our study corroborates and extends work that showed that AAV-mediated Ang1 gene therapy could suppress vascular leakage in stroke (47) and intravitreal recombinant COMP-Ang1 protein could suppress vascular leakage in choroidal neovascularization (48). Our results advance the field by *1*) demonstrating that sustainable delivery of COMP-Ang1 to the retina can be achieved with a single intravitreal injection, *2*) testing the therapeutic effects of COMP-Ang1 in an animal model of DR, and *3*) introducing the potential for COMP-Ang1 to be used in conjunction with ECFCs for the treatment of advanced DR.

In addition, our data raise a number of intriguing questions about the mechanism of action for COMP-Ang1 in DR. Intriguingly, we found that both diabetic and nondiabetic mice experienced decreases in VEGF production due to COMP-Ang1 exposure, inviting inquiry about the nature of this relationship and how it is intertwined with oxygen supply and macrophage secretion (48). Equally fascinating, and consistent with evidence of Ang1 neuroprotection in the central nervous system (49), was our discovery that COMP-Ang1 seems to preserve peripheral RGC density. Ins2Akita mice

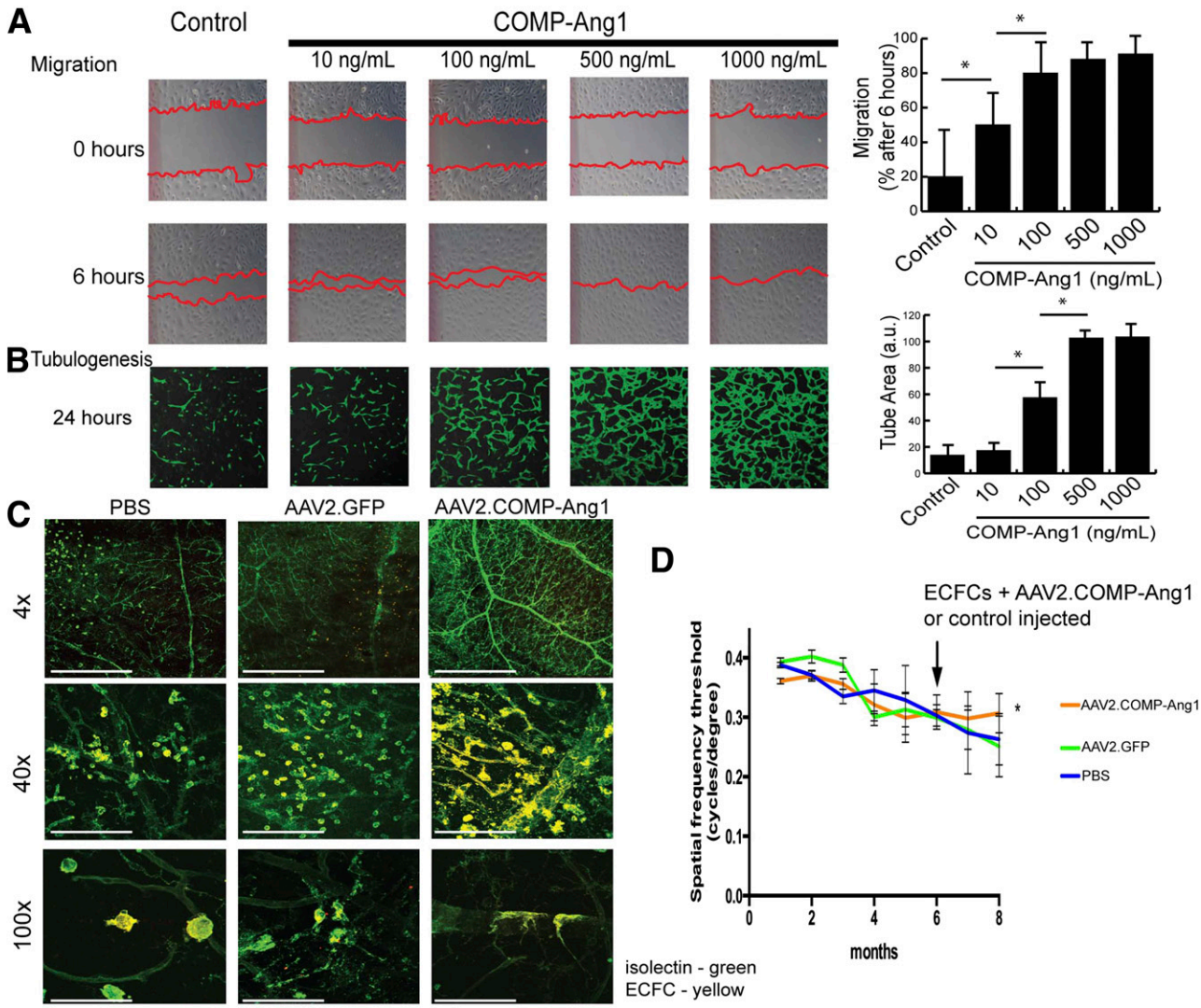

Figure 6—AAV2.COMP-Ang1 enhances ECFC engraftment into the diabetic retina and prevents further visual decline. *A*: ECFCs were plated on collagen-coated wells and assayed for migration potential under increasing doses of COMP-Ang1. *B*: Additionally, three-dimensional tube formation was tested in matrigel. COMP-Ang1 increased migration and tube formation in a dose-dependent manner with maximal effects exerted at 500 ng/mL. Qdot-655–labeled ECFCs were injected intravitreally into aged diabetic mice (6 months [arrow in *D*]) after the mice had been treated with COMP-Ang1 or control. Three days later, retinas were harvested and stained for blood vessels (isolectin 546) and flat mounted for confocal analysis. COMP-Ang1 increased ECFC integration into the diabetic retinal vasculature. *D*: Mice treated with COMP-Ang1 or control plus ECFCs were analyzed for visual tracking ability. COMP-Ang1 plus ECFCs prevented further declines in spatial frequency threshold. *$P < 0.001$ in vitro experiments were performed in triplicate on three different ECFC clones (total of nine experiments per condition). In vivo experiments were performed on five mice per group (10 eyes). Scale bars (*C*): 600 μm (top), 150 μm (middle), and 90 μm (bottom). *$P < 0.01$, ANOVA. Post hoc comparisons with a Tukey test to compare means of each group. a.u., arbitrary units.

reportedly lose RGCs in the peripheral, but not central, retina within 3 months of developing diabetes (41). We speculate this geographic predilection for both RGC apoptosis and COMP-Ang1 rescue may be tied to the concept of increased vulnerability to hypoxia with distance from the central artery, along with our finding that COMP-Ang1 reduces hypoxia. Moreover, since RGCs accounted for only 50–55% of the GC-IPL cell density conserved by COMP-Ang1 in our study, an exploration into other neuroretinal cell types (e.g., cholinergic amacrine cells [50]) as targets for COMP-Ang1 rescue is merited.

We have shown here that COMP-Ang1 is a safe and effective replacement for endogenous Ang1, which can adequately compensate for deficient Ang1 secretion by pericytes. Our results thus far indicate that COMP-Ang1 suppresses the pathognomonic features of nonproliferative DR and, in contrast to existing therapies, decreases the nonperfusion and ischemia critical to the genesis of proliferative DR. This latter finding, along with the long-term duration of action for a single intravitreal injection of AAV2.COMP-Ang1 relative to anti-VEGF agents, holds immense promise for fulfilling an unmet need in the

management of DR if COMP-Ang1 can be successfully translated from the bench to the bedside. Future research will focus on investigating the mechanism of action by which COMP-Ang1 safeguards the retina and the application of COMP-Ang1 to human models of DR.

Acknowledgments. The authors thank Srinivas P. Sangly (Indiana Clinical and Translational Sciences Institute), Jayakrishna Ambati (University of Kentucky), and Valeria Tarallo and Derick Holt (University of Utah) for insightful and constructive discussions. The authors also acknowledge Andrew Weyrich, Guy Zimmerman, and Robert Campbell from the University of Utah for isolating leukocytes.

Funding. This work was partly supported by National Eye Institute, National Institutes of Health, grants 5R01EY017950, 5R01EY017182, and P30EY14800; the University of Utah T-32 Neuroscience Training grant 5T32DC008553-05; the University of Utah Metabolism T-32 Training grant 5T32-DK-091317; James A. Haley Veterans' Hospital (the VA SPIRE: 5 I21 RX001597-02); the Diabetes Research Center at Washington University in St. Louis (grant 5 P30 DK-020579); and the University of Utah Diabetes and Metabolism Center seed grant. This work was also supported in part by an unrestricted grant from Research to Prevent Blindness, Inc., New York, NY, to the Department of Ophthalmology and Visual Sciences, University of Utah.

Duality of Interest. J.M.C., H.U., and B.K.A. have filed a provisional patent application relating to the content of this article. No other potential conflicts of interest relevant to this article were reported.

Author Contributions. J.M.C., R.R.R., L.S.C., H.U., X.Z., C.L.O., R.J.M., P.R.O., S.N., M.M.F., and W.B.M. performed animal studies. J.M.C., R.R.R., H.U., K.W., and A.W.S. performed cell culture studies. J.M.C., R.R.R., P.R.O., W.B.M., P.B., and D.K. performed visual functional studies. J.M.C., K.W., B.J.A., C.C.G., and D.Y.L. performed transendothelial electrical resistance studies. H.U., G.Y.K., and G.G. developed the plasmids and viral vectors. S.K.D. and S.K.M. were responsible for in situ hybridization. J.M.C., R.R.R., L.S.C., B.J.A., and B.K.A. prepared and wrote the manuscript. B.K.A. is the guarantor of this work and, as such, had full access to all the data in the study and takes responsibility for the integrity of the data and the accuracy of the data analysis.

References

1. Yau JWY, Rogers SL, Kawasaki R, et al.; Meta-Analysis for Eye Disease (META-EYE) Study Group. Global prevalence and major risk factors of diabetic retinopathy. Diabetes Care 2012;35:556–564

2. Wild S, Roglic G, Green A, Sicree R, King H. Global prevalence of diabetes: estimates for the year 2000 and projections for 2030. Diabetes Care 2004;27:1047–1053

3. Frank RN. Diabetic retinopathy. N Engl J Med 2004;350:48–58

4. Agarwal A, Sarwar S, Sepah YJ, Nguyen QD. What have we learnt about the management of diabetic macular edema in the antivascular endothelial growth factor and corticosteroid era? Curr Opin Ophthalmol 2015;26:177–183

5. Mitchell P, Bandello F, Schmidt-Erfurth U, et al.; RESTORE study group. The RESTORE study: ranibizumab monotherapy or combined with laser versus laser monotherapy for diabetic macular edema. Ophthalmology 2011;118:615–625

6. Heier JS, Boyer D, Nguyen QD, et al.; CLEAR-IT 2 Investigators. The 1-year results of CLEAR-IT 2, a phase 2 study of vascular endothelial growth factor trap-eye dosed as-needed after 12-week fixed dosing. Ophthalmology 2011;118:1098–1106

7. Campochiaro PA, Wykoff CC, Shapiro H, Rubio RG, Ehrlich JS. Neutralization of vascular endothelial growth factor slows progression of retinal nonperfusion in patients with diabetic macular edema. Ophthalmology 2014;121:1783–1789

8. Elman MJ, Aiello LP, Beck RW, et al.; Diabetic Retinopathy Clinical Research Network. Randomized trial evaluating ranibizumab plus prompt or deferred laser or triamcinolone plus prompt laser for diabetic macular edema. Ophthalmology 2010;117:1064–1077.e35

9. Dornan T, Mann JI, Turner R. Factors protective against retinopathy in insulin-dependent diabetics free of retinopathy for 30 years. Br Med J (Clin Res Ed) 1982;285:1073–1077

10. Joussen AM, Murata T, Tsujikawa A, Kirchhof B, Bursell SE, Adamis AP. Leukocyte-mediated endothelial cell injury and death in the diabetic retina. Am J Pathol 2001;158:147–152

11. Joussen AM, Poulaki V, Le ML, et al. A central role for inflammation in the pathogenesis of diabetic retinopathy. FASEB J 2004;18:1450–1452

12. Mizutani M, Kern TS, Lorenzi M. Accelerated death of retinal microvascular cells in human and experimental diabetic retinopathy. J Clin Invest 1996;97:2883–2890

13. Hammes H-P, Lin J, Wagner P, et al. Angiopoietin-2 causes pericyte dropout in the normal retina: evidence for involvement in diabetic retinopathy. Diabetes 2004;53:1104–1110

14. van Dijk HW, Kok PHB, Garvin M, et al. Selective loss of inner retinal layer thickness in type 1 diabetic patients with minimal diabetic retinopathy. Invest Ophthalmol Vis Sci 2009;50:3404–3409

15. Patel JI, Hykin PG, Gregor ZJ, Boulton M, Cree IA. Angiopoietin concentrations in diabetic retinopathy. Br J Ophthalmol 2005;89:480–483

16. Gavard J, Patel V, Gutkind JS. Angiopoietin-1 prevents VEGF-induced endothelial permeability by sequestering Src through mDia. Dev Cell 2008;14:25–36

17. Thurston G, Rudge JS, Ioffe E, et al. Angiopoietin-1 protects the adult vasculature against plasma leakage. Nat Med 2000;6:460–463

18. Augustin HG, Koh GY, Thurston G, Alitalo K. Control of vascular morphogenesis and homeostasis through the angiopoietin-Tie system. Nat Rev Mol Cell Biol 2009;10:165–177

19. Joussen AM, Poulaki V, Tsujikawa A, et al. Suppression of diabetic retinopathy with angiopoietin-1. Am J Pathol 2002;160:1683–1693

20. Cho C-H, Kammerer RA, Lee HJ, et al. COMP-Ang1: a designed angiopoietin-1 variant with nonleaky angiogenic activity. Proc Natl Acad Sci U S A 2004;101:5547–5552

21. Syrjälä SO, Nykänen AI, Tuuminen R, et al. Donor heart treatment with COMP-Ang1 limits ischemia-reperfusion injury and rejection of cardiac allografts. Am J Transplant 2015;15:2075–2084

22. Moon HE, Byun K, Park HW, et al. COMP-Ang1 Potentiates EPC Treatment of Ischemic Brain Injury by Enhancing Angiogenesis Through Activating AKT-mTOR Pathway and Promoting Vascular Migration Through Activating Tie2-FAK Pathway. Exp Neurobiol 2015;24:55–70

23. Kim DH, Jung YJ, Lee AS, et al. COMP-angiopoietin-1 decreases lipopolysaccharide-induced acute kidney injury. Kidney Int 2009;76:1180–1191

24. Barber AJ, Antonetti DA, Kern TS, et al. The Ins2Akita mouse as a model of early retinal complications in diabetes. Invest Ophthalmol Vis Sci 2005;46:2210–2218

25. Han Z, Guo J, Conley SM, Naash MI. Retinal angiogenesis in the Ins2(Akita) mouse model of diabetic retinopathy. Invest Ophthalmol Vis Sci 2013;54:574–584

26. Zhu W, London NR, Gibson CC, et al. Interleukin receptor activates a MYD88-ARNO-ARF6 cascade to disrupt vascular stability. Nature 2012;492:252–255

27. Medina RJ, O'Neill CL, Devine AB, Gardiner TA, Stitt AW. The pleiotropic effects of simvastatin on retinal microvascular endothelium has important implications for ischaemic retinopathies. PLoS One 2008;3:e2584

28. Medina RJ, O'Neill CL, O'Doherty TM, et al. Myeloid angiogenic cells act as alternative M2 macrophages and modulate angiogenesis through interleukin-8. Mol Med 2011;17:1045–1055

29. Simonelli F, Maguire AM, Testa F, et al. Gene therapy for Leber's congenital amaurosis is safe and effective through 1.5 years after vector administration. Mol Ther 2010;18:643–650

30. Zhang X, Das SK, Passi SF, et al. AAV2 delivery of Flt23k intraceptors inhibits murine choroidal neovascularization. Mol Ther 2015;23:226–234

31. Yin L, Greenberg K, Hunter JJ, et al. Intravitreal injection of AAV2 transduces macaque inner retina. Invest Ophthalmol Vis Sci 2011;52:2775–2783
32. Cogan DG, Toussaint D, Kuwabara T. Retinal vascular patterns. IV. Diabetic retinopathy. Arch Ophthalmol 1961;66:366–378
33. Davis S, Aldrich TH, Jones PF, et al. Isolation of angiopoietin-1, a ligand for the TIE2 receptor, by secretion-trap expression cloning. Cell 1996;87:1161–1169
34. Uemura A, Ogawa M, Hirashima M, et al. Recombinant angiopoietin-1 restores higher-order architecture of growing blood vessels in mice in the absence of mural cells. J Clin Invest 2002;110:1619–1628
35. Thurston G. Complementary actions of VEGF and angiopoietin-1 on blood vessel growth and leakage. J Anat 2002;200:575–580
36. Huang H, Gandhi JK, Zhong X, et al. TNFalpha is required for late BRB breakdown in diabetic retinopathy, and its inhibition prevents leukostasis and protects vessels and neurons from apoptosis. Invest Ophthalmol Vis Sci 2011;52:1336–1344
37. Chibber R, Ben-Mahmud BM, Chibber S, Kohner EM. Leukocytes in diabetic retinopathy. Curr Diabetes Rev 2007;3:3–14
38. Vinores SA, Xiao W-H, Shen J, Campochiaro PA. TNF-alpha is critical for ischemia-induced leukostasis, but not retinal neovascularization nor VEGF-induced leakage. J Neuroimmunol 2007;182:73–79
39. Cahoon JM, Olson PR, Nielson S, et al. Acridine orange leukocyte fluorography in mice. Exp Eye Res 2014;120:15–19
40. Miyamoto K, Khosrof S, Bursell SE, et al. Vascular endothelial growth factor (VEGF)-induced retinal vascular permeability is mediated by intercellular adhesion molecule-1 (ICAM-1). Am J Pathol 2000;156:1733–1739
41. Gastinger MJ, Kunselman AR, Conboy EE, Bronson SK, Barber AJ. Dendrite remodeling and other abnormalities in the retinal ganglion cells of Ins2 Akita diabetic mice. Invest Ophthalmol Vis Sci 2008;49:2635–2642
42. Aung MH, Kim MK, Olson DE, Thule PM, Pardue MT. Early visual deficits in streptozotocin-induced diabetic long evans rats. Invest Ophthalmol Vis Sci 2013;54:1370–1377
43. Hombrebueno JR, Chen M, Penalva RG, Xu H. Loss of synaptic connectivity, particularly in second order neurons is a key feature of diabetic retinal neuropathy in the Ins2Akita mouse. PLoS One 2014;9:e97970
44. Caballero S, Hazra S, Bhatwadekar A, et al. Circulating mononuclear progenitor cells: differential roles for subpopulations in repair of retinal vascular injury. 2013;54:3000–3009
45. Medina RJ, O'Neill CL, Humphreys MW, Gardiner TA, Stitt AW. Outgrowth endothelial cells: characterization and their potential for reversing ischemic retinopathy. Invest Ophthalmol Vis Sci 2010;51:5906–5913
46. Medina RJ, O'Neill CL, Sweeney M, et al. Molecular analysis of endothelial progenitor cell (EPC) subtypes reveals two distinct cell populations with different identities. BMC Med Genomics 2010;3:18
47. Shen F, Walker EJ, Jiang L, et al. Coexpression of angiopoietin-1 with VEGF increases the structural integrity of the blood-brain barrier and reduces atrophy volume. J Cereb Blood Flow Metab 2011;31:2343–2351
48. Lee J, Kim KE, Choi D-K, et al. Angiopoietin-1 guides directional angiogenesis through integrin $\alpha v\beta 5$ signaling for recovery of ischemic retinopathy. Sci Transl Med 2013;5:203ra127–7
49. Shin HY, Lee YJ, Kim HJ, et al. Protective role of COMP-Ang1 in ischemic rat brain. J Neurosci Res 2010;88:1052–1063
50. Gastinger MJ, Singh RSJ, Barber AJ. Loss of cholinergic and dopaminergic amacrine cells in streptozotocin-diabetic rat and Ins2Akita-diabetic mouse retinas. Invest Ophthalmol Vis Sci 2006;47:3143–3150